Evidence from electrical transport and photoluminescence spectroscopy of a band of localized deep donors in high-purity *n*-type InP grown by chemical-beam epitaxy

R. Benzaquen*
Institute for Microstructural Sciences, National Research Council of Canada, Ottawa, Ontario, Canada K1K 0R6

M. Benzaquen†
Centre for Advanced Materials and Related Technologies, Department of Mechanical Engineering, University of Victoria, P.O. Box 3055, Victoria, British Columbia, Canada V8W 3P6

S. Charbonneau, P. J. Poole, T. Sudersena Rao, C. Lacelle, and A. P. Roth*
Institute for Microstructural Sciences, National Research Council of Canada, Ottawa, Ontario, Canada K1K 0R6

R. Leonelli
Département de Physique et Groupe de Recherche en Physique et Technologie des Couches Minces, Université de Montréal, Case Postale 6128, Succursale A, Montréal, Québec, Canada H3C 3J7

(Received 12 May 1994)

We have measured the Hall mobility and Hall electronic concentration as a function of temperature of three low-compensation *n*-type InP epilayers of similar thickness grown by chemical-beam epitaxy. The Hall mobility of the samples was found to be exceptionally high at 77 K and significantly depressed at 300 K. Above the freeze-out region, strong Hall electronic excitation was consistently observed in the temperature range of $\approx 35-300$ K. These features are in excellent agreement with a model accounting for a broad band of localized deep-donor centers or complexes of unknown origin, centered at 160 meV below the conduction band. In addition, all samples showed an anomalous metal-like behavior at the lowest temperatures, instead of the expected strong localization regime. A broad luminescent band of ≈ 11-meV linewidth linked to the presence of the band of deep donors was observed below the acceptor bound-exciton transition. Time-resolved photoluminescence and photoluminescence-excitation measurements supported the bound-exciton nature of the luminescent band.

I. INTRODUCTION

In *n*-type InP, the simultaneous observation of a high-temperature (T) increase in the Hall electronic concentration (n_H) and of a reduced Hall mobility (μ_H) at 300 K, despite high values of the low-T μ_H, has been interpreted on the basis of a deep center or complex with 80- or 160-meV binding energy.[1-3] These features are general electrical characteristics of epitaxial *n*-type InP grown by metal-organic vapor-phase epitaxy (MOVPE). In contrast, the samples grown by chemical-beam epitaxy (CBE) investigated in this work show a different behavior of n_H versus T. It is observed that n_H strongly increases in a broad T range ($\approx 35-300$ K) without showing any saturation effect. This behavior may be explained on the basis of a shallow donor with 7-meV binding energy and a broad distribution of localized deep donors, with finite width, centered at 160 meV below the conduction band. Following a general practice,[4] we use the term "band" to denote this distribution. As T increases and the Fermi level E_F falls deeper into the band of deep donors, the deep centers start to ionize and provide additional electronic excitation to the conduction band. They then also act as strong scatterers and very significantly reduce μ_H in a broad T range.

Photoluminescence (PL) measurements were carried out that confirm the presence of the deep-donor band. A broad luminescent band of ≈ 11-meV linewidth was observed below the acceptor bound-exciton (A^0,X) transition in our *n*-type InP samples. Künzel and Ploog[5] observed in the corresponding spectral range of nominally undoped *p*-type GaAs layers grown by molecular-beam epitaxy, a series of defect-related PL lines (so-called KP lines). Subsequently, strong evidence was provided for the (A^0,X) nature of these KP lines,[6] and of a direct link between these lines and their corresponding free-to-bound and donor acceptor pair transitions. Although no sharp lines are observed in this spectral region in our *n*-type InP samples, photoluminescence excitation (PLE) and time-resolved photoluminescence (TRPL) measurements support the bound-exciton nature of the luminescent band. The binding energies of the deep centers extracted from the optical measurements are consistent with the values deduced from the analysis of the electrical transport data.

II. EXPERIMENTS

The InP epilayers were grown by CBE on (100) semi-insulating Fe-doped InP substrates using phosphine (PH_3) and triethylindium. Details about the growth conditions are given elsewhere.[7] All the layers had a thickness of 5

μm measured using a scanning electron microscope or an electrochemical profiler. Resistivity measurements indicated excellent uniformity across the area of the sample. Hall effect measurements were conducted in the T range of 4.2–300 K under low electric and magnetic field conditions using a Van der Pauw configuration. The samples were in good thermal contact with a copper block in which a carbon glass temperature sensor was embedded, allowing a precision of 0.01 K at the lowest T. To avoid gradient effects, the temperature recovered without heat supply from its lowest value at a very slow rate. The data were collected with a high-resolution automated data acquisition system which allows data points to be acquired at intervals of 0.05 K. The measurements were performed under low electric field (F) conditions in the whole T range, as verified by the linearity of the current-voltage I-V characteristics of the samples. This required frequent adjustments of the excitation current as T was changing. Low magnetic-field (B) conditions could not be preserved at low T despite a constant value of 0.47 kG.

The optical measurements were carried out in a liquid-He bath cryostat with the samples mounted strain-free on a Cu block. The PL and PLE spectra were taken using a HeNe or a Ti:Sa tunable laser pumped by an Ar^+ laser. The luminescence was dispersed by a double 0.75-m spectrometer or by a 0.64-m spectrometer and detected by an imaging photomultiplier tube or by a liquid-N_2-cooled charge coupled device, providing in both cases a resolution of ≈ 0.04 meV. The pulse excitation for the TRPL experiments was provided by a mode-locked Nd^{3+}:YAG (yttrium aluminum garnet) laser synchronously pumping a R640 dye laser. The resulting 5-ps pulses were at a wavelength of 620 nm and the repetition rate was 4 MHz. The transient PL measurements were carried out using a delayed coincidence photon-counting system. The instrumental response of this system had an exponential decay time constant of 100 ps. The excitation power density was set at ≈ 1.5 W/cm^2 for all the optical experiments.

III. ELECTRICAL TRANSPORT ANALYSIS

The analysis of the data uses one of the iterative solutions to the Boltzmann equation derived by Rode.[8,9] This method allows the calculation of μ_H for fixed values of F and B. It includes nonparabolicity corrections for the conduction band and its coupling with the light-hole valence band. This coupling is obtained by admixture of p-type wave functions in the scattering processes, which leads to an overlap integral appearing as an additional factor in the different elastic scattering rates. The elastic scattering mechanisms considered in this work are ionized impurity,[10] screened piezoelectric,[11] deformation potential acoustic,[12] and neutral impurity.[13] The expressions of the corresponding relaxation times were used as modified by Rode[12] to include admixture of valence-band wave functions. Polar optical-phonon scattering is then taken into account by the Rode[12] iterative technique.

The Hall mobility is given by[2,9]

$$\mu_H = \frac{\int_0^\infty k^3 \frac{h(k)}{Bd} dk}{\int_0^\infty k^3 \frac{g(k)}{d} dk} , \tag{1}$$

where $g(k)$ is the perturbation of the Fermi-Dirac distribution function F_0 due to F in the presence of B, while $h(k)$ represents the perturbation of F_0 due to B. These perturbations are the solution of a set of two coupled finite difference equations.[2] k is the electronic wave vector and d is a function of k that can be viewed as an effective-mass correction linked to nonparabolicity.[2,12] $g(k)$ and $h(k)$ define a convergent iterative procedure suitable for a numerical treatment.[2] This technique requires the evaluation of the functions $g(k^{\pm})$ and $h(k^{\pm})$. $k^{\pm}$ is the wave vector corresponding to the energy $E \pm k_B T_0$, where k_B is the Boltzmann constant and T_0 the temperature of the polar optical phonons. In practice, the iterative procedure has been halted when the average relative variation of $g(k)$ and $h(k)$ fell below 1%.

In a similar way, the drift mobility μ is given by[2,12]

$$\mu = \frac{\hbar}{3m} \frac{\int_0^\infty k^3 \frac{p(k)}{Fd} dk}{\int_0^\infty k^2 F_0 dk} , \tag{2}$$

where m represents the free-electron mass, and $p(k)$ is the perturbation of F_0 due to F when no B is applied. $p(k)$ is obtained as the numerical solution of another finite-difference equation.[2]

The Hall factor r_H is then defined by

$$r_H = \frac{\mu_H}{\mu} \tag{3}$$

which yields

$$n_H = \frac{n_c}{r_H} , \tag{4}$$

n_c being the concentration of free electrons in the conduction band, given by the neutrality equation

$$n_c = N_{D_1}^+ + N_{D_2}^+ - N_A , \tag{5}$$

with

$$N_{D_1}^+ = \frac{N_{D_1}}{1 + \frac{1}{\beta_{D_1}} \exp\left[\frac{E_F - E_{D_1}}{k_B T}\right]} , \tag{6a}$$

$$N_{D_2}^+ = N_{D_2} - n_{D_2} , \tag{6b}$$

$$n_{D_2} = \int_{-\infty}^{\infty} G_{D_2}(E) F_0(E) dE , \tag{6c}$$

$$G_{D_2}(E) = \frac{N_{D_2}}{\sqrt{2\pi}\sigma_{D_2}} \exp\left[-\frac{1}{2}\left[\frac{E - E_{D_2^c}}{\sigma_{D_2}}\right]^2\right] , \tag{6d}$$

where N_A, N_{D_1}, and N_{D_2} are, respectively, the concentration of acceptors, shallow donors, and deep donors. E_{D_1} is the shallow-donor binding energy with degeneracy fac-

tor β_{D_1}. The superscript + denotes the ionized donors. n_{D_2} represents the electronic concentration of localized deep donors, while $G_{D_2}(E)$ is the corresponding density of states, taken as a first approximation of a Gaussian centered at $E_{D_2^c}$ and normalized to N_{D_2}. σ_{D_2} is the standard deviation of the Gaussian distribution. The expression of n_c used in this work includes nonparabolicity corrections of the conduction band and is given by

$$n_c = \int_{E_c}^{\infty} G_c(E) F_0(E) dE \ , \tag{7}$$

where E_c is the bottom of the conduction band, and $G_c(E)$ the corresponding density of states given by[2]

$$G_c(E) = \frac{4md}{h^2} k \ . \tag{8}$$

Equation (5), with $N_{D_1}^+$, $N_{D_2}^+$, and n_c, respectively, given by Eqs. (6a), (6b), and (7) can then be solved numerically for E_F, as a function of T, without further approximation.

Deep centers affect electronic transport in two very different ways. When they are neutral, they are weaker scatterers than neutral shallow impurities.[2,3] Consequently, as in a previous work, we neglect scattering by neutral deep centers, and only consider the neutral shallow donors.[2,3] The concentration N_N of neutral scatterers is taken as

$$N_N = N_{D_1} - N_{D_1}^+ = \frac{N_{D_1}}{1 + \beta_{D_1} \exp\left[\dfrac{E_{D_1} - E_F}{k_B T}\right]} \ . \tag{9}$$

On the other hand, when they become ionized, deep centers, due to their hard-core potential, are known to be very strong scatterers.[14] In this model, we account for the deep centers using a simple spherical square-well potential of the form

$$V(r) = \begin{cases} V_0, & r \le a \\ 0, & r > a \ , \end{cases} \tag{10}$$

where a is the radius of the well and V_0 is its negative depth. Although the potential of Eq. (10) is unphysical, it has been proven to be equivalent, regarding scattering, to a more realistic hard-core screened potential.[1,14,15] The relaxation time associated with the scattering by this well is given by[1]

$$\frac{1}{\tau_w} = \frac{4\pi\hbar N_{D_2}^+}{m^* k} \sum_{L=0}^{\infty} (L+1) \sin^2(\delta_L - \delta_{L+1}) \ , \tag{11}$$

where m^* is the electron effective mass. The successive phase shifts δ_L of Eq. (11) can be calculated to any order using an iterative procedure.[1] τ_w is then a function of the energy of the incident electron E, V_0, and a. In practice, the iterations were halted when the relative variation between successive δ_L fell below 10^{-6}. If we set in a first approximation $V_0 = E_{D_2^c}$, the full model for n_H and μ_H requires the five parameters N_{D_1}, N_{D_2}, N_A, σ_{D_2}, and a. Regarding the fitting procedure, the set of parameters N_{D_1} and N_A can be determined independently from the others by using the variations of n_H and μ_H in the temperature range of 4.2–35 K, where the deep centers are still neutral and electrically inactive. This first procedure only requires one parameter per independent curve. Two independent experimental curves are available for the three remaining parameters N_{D_2}, σ_{D_2}, and a, namely, $\mu_H(T)$ and $n_H(T)$, which show large variations in a broad T range (35–300 K) covering several conduction regimes. In addition, the theoretical curves are very sensitive to the variations of particular parameters within specific T ranges. These parameters can consequently be accurately determined using adequate physical considerations. The physical parameters of InP used in the model are given in Table I and are well established from independent measurements.[1,12,16]

Figure 1 shows the behavior of μ_H (full inverted triangles) and n_H (open inverted triangles) for sample 1 as a function of T. The value of μ_H around 50 K (over 300 000 $\mathrm{cm^2\,V^{-1}\,s^{-1}}$) is exceptionally high for an InP sample grown by CBE and seems to indicate a sample of very high purity. Nevertheless, the fast increase of $n_H(T)$ observed above $\approx$35 K indicates strong excitation to the conduction band in a T range where the saturation of n_c is generally expected. This electronic excitation to the conduction band is attributed to the ionization of a band of deep donors. The procedure for fitting our model to the data requires some discussion. The procedure for determining N_{D_1} and N_A is well established for samples without deep donors. In such a case, a single experimental point of $\mu_H(T)$ and $n_H(T)$ is generally sufficient at 77 K: the difference $N_{D_1} - N_A$ is varied until agreement is

TABLE I. Physical parameters of InP used in the computation. m^* is the electron effective mass, ϵ_s and ϵ_∞ are, respectively, the low and high dielectric constants. T_{po} is the temperature of the polar-optical phonons. ρ_m is the mass density, E_1 is the acoustical deformation potential, C_L is the longitudinal speed of sound, and P is the piezoelectric coefficient. E_{D_1} is the shallow-donor binding energy. $E_{D_1^c}$ is the binding energy corresponding to the center of the deep-donor band. $E_g(0)$ is the 0-K band gap, l and R are, respectively, the coefficients of thermal expansion and compressibility and $(\partial E_g/\partial P)_T$ is the variation of band gap with pressure.

m^* (a.u.)	0.082
ϵ_s	12.38
ϵ_∞	9.55
T_{po} (K)	497
ρ_m (g/cm^3)	4.487
E_1 (eV)	6.8
C_L (cm/s)	5.028×10^5
P	0.013
E_{D_1} (meV)	7
$E_{D_2^c}$ (meV)	160
$E_g(0)$ (eV)	1.42
$\frac{3l}{R}\left[\frac{\partial E_g}{\partial P}\right]_T$ (eV/K)	5×10^{-5}

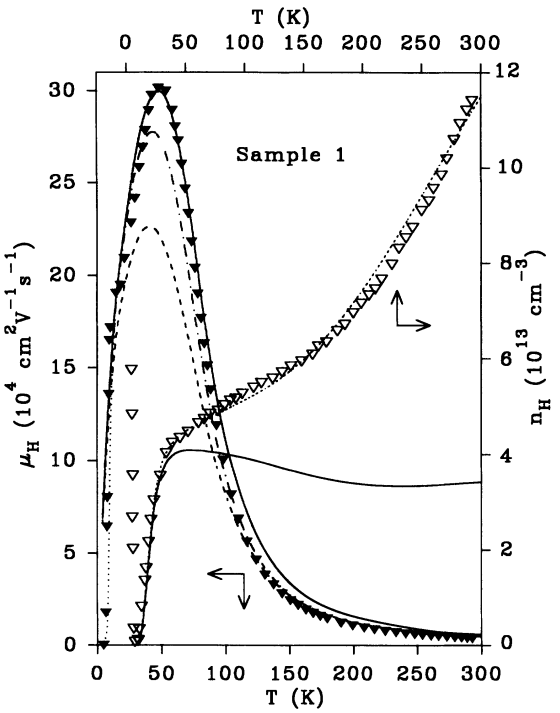

FIG. 1. Hall mobility (inverted full triangles) and Hall electronic concentration (inverted open triangles) of sample 1 as a function of temperature. The solid curve is the fit of the model to the data when a deep donor band is not accounted for. The dashed curve is obtained when a deep donor band is accounted for. The dashed-dotted curve is obtained when the deep donor band is divided into 50 narrow energy intervals. The dashed and dashed-dotted curves do not modify the calculation of the Hall electronic concentration. The dotted curve corresponds to the inclusion of impurity conduction.

obtained between theory and experiment, for n_H, at 77 K; N_{D_1} and N_A are then simultaneously varied, keeping the difference $N_{D_1}-N_A$ constant, until agreement is reached with the experimental μ_H. When deep donors are present, their specific effects must be clearly separated from the effects of the shallow donors. This occurs, for example, when all shallow donors are ionized while the deep centers are still neutral. In such a T range, n_H should be relatively flat. In the present situation, there is no T range where n_H is constant, and consequently the shallow donors are never totally ionized while the deep centers are all still neutral, and thus electrically inactive. Nevertheless, at low enough T, when most of the deep centers are still neutral, their effects should be negligible and electrical conduction should be dominated by the shallow donors. Within such a T range, the analysis of the data should be identical to the case where no deep centers are present, and should allow an independent determination of N_{D_1} and N_A. We note that the onset of excitation of the deep center occurs at a T value lower than the one at which μ_H peaks. Thus, the deep centers start to be electrically active before μ_H reaches its maximum value. It is then expected, in addition to the usual

TABLE II. Results obtained from the analysis of three InP samples. N_{D_1}, N_{D_2}, and N_A are, respectively, the shallow donor, deep donor, and acceptor concentrations; σ_{D_2} is the standard deviation of the band of deep donors. a is the radius of the well. n_{D_1} and μ_{D_1} are, respectively, the electronic concentration and mobility in the impurity band. β_{D_1} is the degeneracy factor for the shallow donors.

Sample No.	N_{D_1} (cm^{-3})	N_{D_2} (cm^{-3})	N_A (cm^{-3})	σ_{D_2} (meV)
1	7.9×10^{13}	1.39×10^{14}	3.7×10^{13}	70
2	1.38×10^{14}	2.0×10^{14}	7.3×10^{13}	65
3	1.82×10^{14}	1.45×10^{14}	6.8×10^{13}	75

Sample No.	μ_{D_1} (cm^{2}V^{-1}s^{-1})	n_{D_1} (cm^{-3})	β_{D_1}	a (Å)
1	903	2.9×10^{13}	0.5	800
2	2251	1.21×10^{13}	0.5	800
3	580	1.35×10^{14}	0.5	800

μ_H reduction at high T[1], that the corresponding μ_H at low T will be reduced as well. The solid lines of Fig. 1 have been generated with the physical parameters of InP presented in Table I, with $N_{D_2}=0$ and the values of N_{D_1} and N_A reported in Table II. These two values, which indicate a sample of very high purity, have been obtained with the experimental values of $\mu_H(T)$ and $n_H(T)$ at 25 K using the simple procedure described above. The fits are excellent at relatively low T. Nevertheless, at the lowest T, the theoretical μ_H is significantly larger than the corresponding experimental values. The opposite is observed for the theoretical n_H, which falls below experiment. Both effects, which are linked to the increase of n_H with decreasing T, are known to be due to impurity conduction at the lowest T, and will be considered later. A large discrepancy between theory and experiment is observed for n_H above $\approx$35 K, reaching a factor 3 at 300 K. At 300 K, the calculated value of μ_H is 6000 cm^{2}V^{-1}s^{-1}, which is the theoretical limit of μ_H in InP. The corresponding experimental value of 4435 cm^{2}V^{-1}s^{-1} is smaller. These two effects can be taken into account by including a band of deep donors in the model. Assuming, on the basis of a previous work,[1] that this band is centered at 160 meV below the conduction band, three parameters, namely, N_{D_2}, σ_{D_2}, and a, have to be determined from $\mu_H(T)$ and $n_H(T)$ in the T range of $\approx$35–300 K (noticing that this deep-donor band has no effect on low-T data). The fitting procedure was based on the following considerations. The startup of excitation to the conduction band (35 K for sample 1) was only weakly affected by variations of both N_{D_2} and σ_{D_2}. N_{D_2} appeared to control the values of n_H at the highest T. We also found that σ_{D_2}, which is a measure of the width of the band, mainly controls the curvature of $n_H(T)$ in the T range under consideration. Consequently, N_{D_2} was varied until agreement with n_H at 300 K was achieved. σ_{D_2} was subsequently adjusted in order to reach agree-

ment with n_H at 170 K. Finally, the radius a of the spherical square well was varied to obtain agreement with μ_H at 300 K. The results of the fit are the dashed lines of Fig. 1. The parameters extracted from the fitting procedure are reported in Table II, and show a low level of compensation when the compensation is taken as $N_A/(N_{D_1}+N_{D_2})$. Moreover, N_{D_2} is much larger than N_{D_1}. It is thus clear that the low-T μ_H is not a measure of the purity of this sample. For n_H, the overall agreement between theory and experiment is excellent in the whole T range (except at very low T, where impurity conduction dominates electrical transport). For μ_H, the fit is excellent at high T. However, an important discrepancy of $\approx 25\%$ is observed at low T. This discrepancy occurs around the T region where μ_H peaks, where an important amount of deep centers is already ionized, as evidenced by the behavior of $n_H(T)$. This effect appears to be related to the value of σ_{D_2} quoted in Table II. This value shows that the band of localized deep-donor centers is quite broad and extends up to the edge of the conduction band. Consequently, the condition $\sigma_{D_2} \ll E_{D_2^c}$ is not verified. The approximation $V_0 = E_{D_2^c}$ overestimates the scattering strength of the deep centers associated with the low-energy side of $G_{D_2}(E)$. It also underestimates the scattering strength corresponding to the high-energy side of $G_{D_2}(E)$, which is unlikely to affect μ_H at 300 K, where $n_H(T)$ neither saturates nor shows a change of curvature, indicating that the excitation originates from the low-energy side of $G_{D_2}(E)$. To reduce the discrepancy between theory and experiment observed for μ_H in the T range where the deep centers start to ionize and to act as scatterers, it is necessary to consider the scattering effects of the band at every energy. Instead of assuming a unique depth for the square-well potentials, the deep-donor band is divided into m narrow energy intervals of width ΔE_i, centered at an energy E_i and corresponding to a concentration of deep ionized centers $N^+_{D_{2_i}}$. Each energy E_i defines the depth of the wells associated with $N^+_{D_{2_i}}$ deep ionized centers: $V_{0_i} = E_i$, $E_{D_2^c} + W < E_i < E_{D_2^c} - W$, $i = 1$ to m, where W is the width at half maximum of the deep-donor band, $W = 2\sqrt{2\ln 2}\,\sigma_{D_2}$. All the wells with a particular depth produce a scattering mechanism associated with a relaxation time of the form of Eq. (11). Consequently, the total relaxation time originating from the whole deep-donor band is given by

$$\frac{1}{\tau_w} = \sum_{i=1}^{m} \frac{1}{\tau_{w_i}} = \frac{4\pi\hbar}{m^* k} \sum_{i=1}^{m} \sum_{L=0}^{\infty} N^+_{D_{2_i}} (L+1)\sin^2(\delta_{i,L} - \delta_{i,L+1}) , \tag{12}$$

with

$$N^+_{D_{2_i}} = \int_{E_i - \Delta E_i/2}^{E_i + \Delta E_i/2} G_{D_2}(E)[1 - F_0(E)]dE \approx G_{D_2}(E_i)[1 - F_0(E_i)]\Delta E_i . \tag{13}$$

Equations (12) and (13) do not modify the calculation $n_H(T)$. They have been implemented numerically with $m = 50$ and the same parameters as in the previous calculation, which increased considerably the computation time. As shown by the dashed-dotted line of Fig. 1, the overall agreement between experimental and theoretical μ_H is now excellent in the whole T range, although a small discrepancy is still noticeable in the region where μ_H peaks. We note that the dashed and the dashed-dotted lines are identical at low T and extremely close from each other at high T. The discrepancy around the peak of μ_H is not accidental, as it is observed for all samples. It occurs when E_F is close to the edge of the low-energy tail of the deep-donor band, when scattering is dominated by relatively shallow wells. In such an energy range, the model overestimates the scattering strength of these relatively shallow centers, indicating the failure of the spherical square-well approximation. The above analysis has also been applied to samples 2 and 3. Figures 2 and 3 display the corresponding results, obtained with the same values of E_{D_1}, $E_{D_2^c}$, and a. These samples were slightly more heavily doped and also lightly compensated. The results of the fit are reported in Table II.

Figure 4 presents the computed values of r_H as a function of T for all three samples, and shows that taking $r_H = 1$ leads to considerable error, in particular at low T. These curves were generated without taking deep centers into account with $B = 0.47$ kG and $F = 30$ mV/cm. The inclusion of deep centers in our model does not change significantly the behavior of r_H versus T. Maximum values of $r_H \approx 1.45$ are obtained for all three samples, the

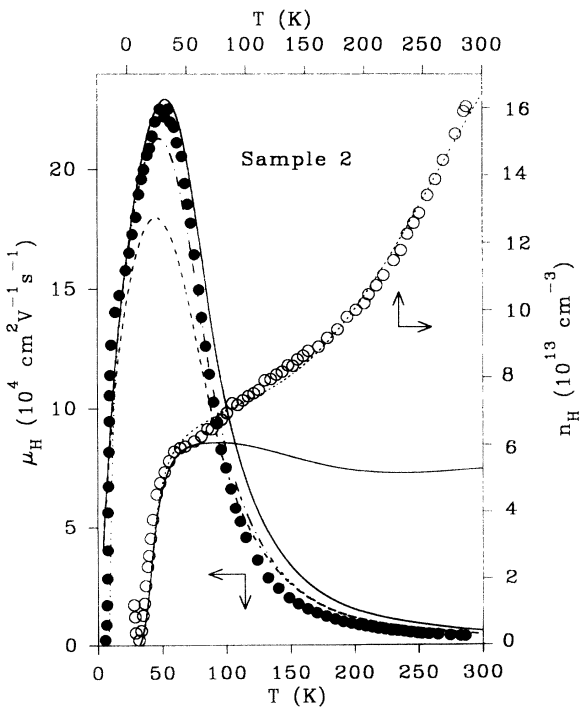

FIG. 2. Hall mobility (full circles) and Hall electronic concentration (open circles) of sample 2 as a function of temperature. The curves are as for Fig. 1.

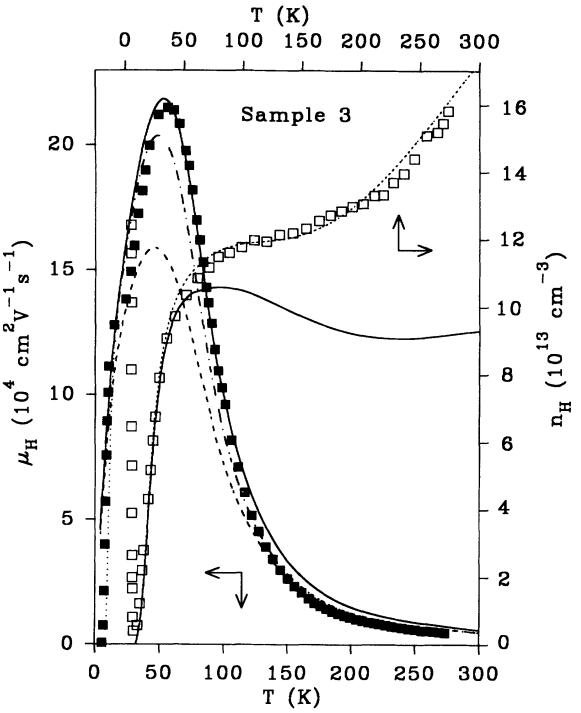

FIG. 3. Hall mobility (full squares) and Hall electronic concentration (open squares) of sample 3 as a function of temperature. The curves are as for Fig. 1.

maximum theoretical value expected for pure ionized scattering being of the order of 1.9,[17] under low B conditions. This can be attributed to an admixture of screened piezoelectric and neutral impurity scattering with ionized impurity scattering. As the mobility of the samples decreases, the low B condition $\mu^2B^2 \ll 1$ is more easily reached. This is evidenced by the departure from approximately unity of the minimum value of r_H as the doping level increases.

Impurity conduction was present at the lowest T, as evidenced by the low T increase of n_H shown in Figs. 1–3. For high-purity samples, the shallow-donor band, which is partly filled due to compensation, is expected to show impurity conduction in the strong localization regime.[4] Figure 5 presents the variations of $\ln[n_H]$ versus $1/T$ for samples 1 (open inverted triangles) and 3 (open squares). The results for sample 2 are similar (not shown). The minimum of n_H observed at low T is well known to be due to two band conduction:[2,3] the conduction band is dominant on the left-hand side of the minimum, the impurity band on the right-hand side. The solid lines correspond to the theoretical $n_H(T)$ when impurity conduction is not taken into account (they correspond to the solid lines of Figs. 1–3). The slopes of these lines give a binding energy of $E_{D_1} = 7$ meV in rather narrow freeze-out regions. Huge discrepancies are observed at the lowest T between experiment and theory. The

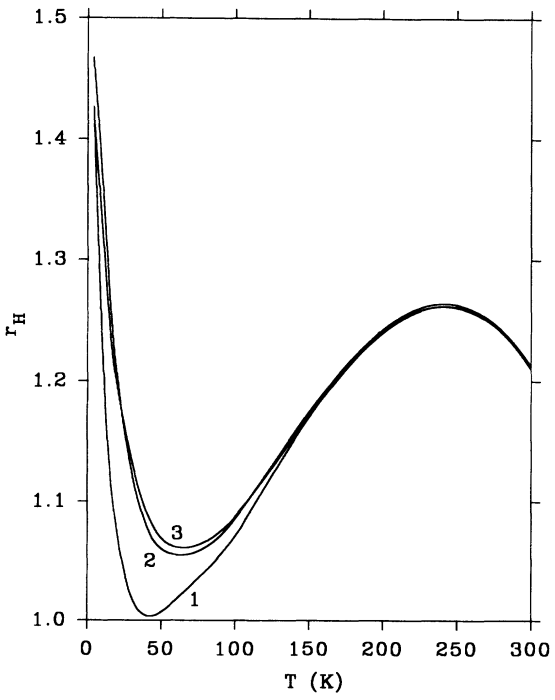

FIG. 4. Hall factor as a function of temperature for samples 1, 2, and 3, respectively.

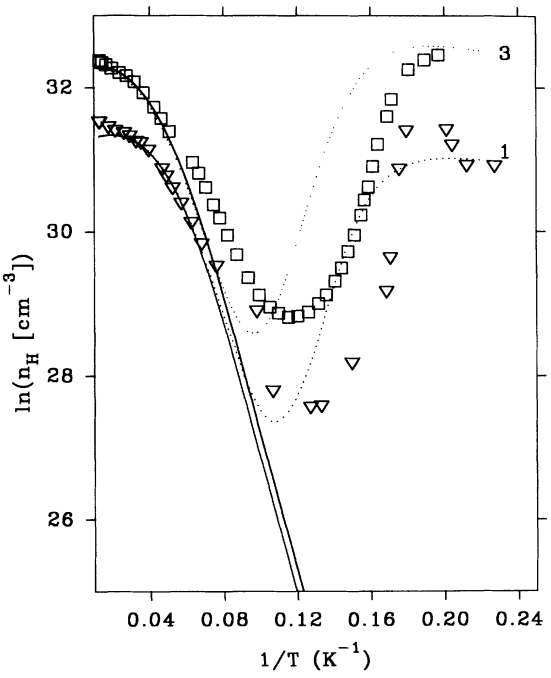

FIG. 5. The logarithm of the Hall electronic concentration as the function of the inverse temperature for samples 1 (inverted open triangles) and 2 (open squares). The solid curve is the full model when the deep-donor band is not accounted for. The dotted curve is obtained when impurity conduction is taken into account.

solid lines are several orders of magnitude below experiment at the lowest T, which indicates very strong impurity conduction. This is related to the fact that the samples exhibited surprisingly low resistance in the impurity conduction region. Evidence of this is provided by the behavior of n_H at the lowest T: $n_H(T)$ tends towards a constant value as T decreases. A similar behavior is observed for μ_H (not shown). This metal-like behavior is totally unexpected for samples of such purity at T values where hopping conduction is generally observed.[4] Nevertheless, this behavior has been observed in several n-type InP epitaxial layers grown by MOVPE.[18] A two-band model is then generally sufficient to explain the general characteristics of the data at the lowest T. When conduction in an impurity band is added to the effects of the conduction band, the combined low T Hall mobility μ_L and electronic concentration n_L are[2]

$$\mu_L = \frac{n_c r_H \mu^2 + n_{D_1} \mu_{D_1}^2}{n_c \mu + n_{D_1} \mu_{D_1}} , \tag{14a}$$

$$n_L = \frac{(n_c \mu + n_{D_1} \mu_{D_1})^2}{n_c r_H \mu^2 + n_{D_1} \mu_{D_1}^2} , \tag{14b}$$

where n_{D_1} and μ_{D_1} are, respectively, the electronic concentration and the mobility in the impurity band. r_H has been taken as 1 for the impurity band. On the basis of previous observations,[2,3] we have assumed constant values for both μ_{D_1} and n_{D_1}, which are quoted in Table II. Equations (14a) and (14b) can then be computed at low T using the curves of $\mu_H(T)$ and $n_H(T)$ previously calculated. In Figs. 1–3, the dotted lines, which are in much better agreement with experiment at very low T, are obtained when impurity conduction is taken into account. Figure 5 shows that the two-band model reproduces fairly well the general characteristics of the low T variations of n_H. The discrepancies observed can be partially corrected by assuming a slow T dependence of n_{D_1} and μ_{D_1}.

IV. OPTICAL ANALYSIS

Figure 6 shows a typical 4.2-K PL spectrum (open circles) of sample 1 obtained by resonantly exciting the $(F,X)_{n=2}$ transition at an excitation power density of ≈ 1.5 W/cm^2, which enhances both the intensity and spectral differentiation of bound excitons. The solid lines are Lorentzian fits centered at the ith observed transition energy $h\nu_i$ of linewidth γ_i. The PL of samples 2 and 3 displays very similar optical features (not shown). As expected the PL spectrum is dominated by intense neutral shallow-donor bound-exciton transitions $(D^0,X)_n$ up to $n=4$ components (structures b–e), followed at higher energy by less intense $(F,X)_{n=1}$ transitions (structure a). However, we note that under nonresonant excitation conditions, the PL spectrum is dominated by intense

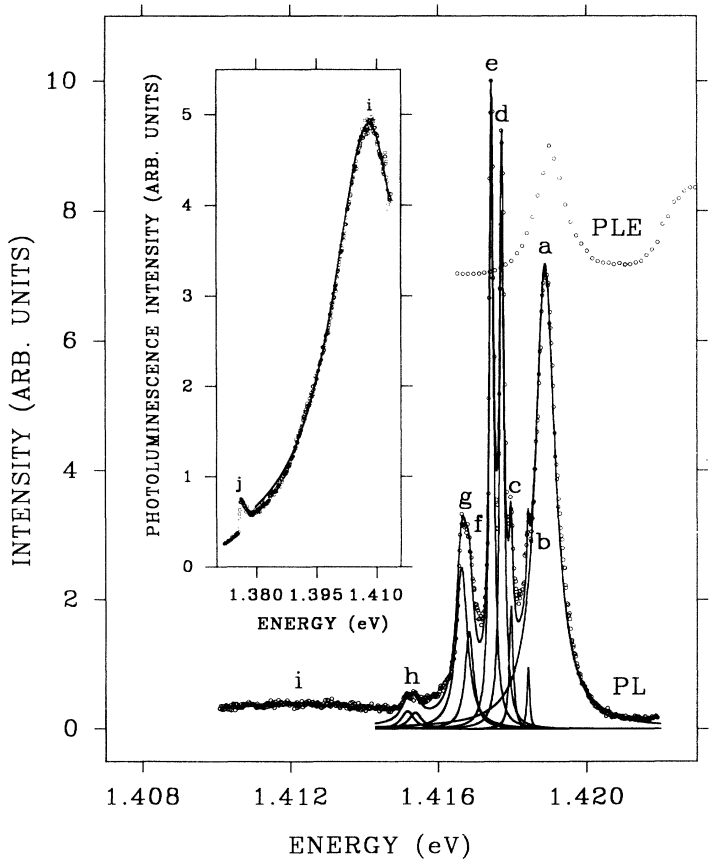

FIG. 6. 4.2-K photoluminescence and photoluminescence-excitation spectra of sample 1 (open circles). The solid curves are Lorentzian fits to the photoluminescence data. $a=(F,X)_{n=1}$ is the $n=1$ free-exciton transition; b, c, d, and e are, respectively, the $n=4$, 3, 2, and 1 neutral shallow donor bound-exciton transitions $(D^0,X)_n$; $f=(D^0,h)$ is the neutral shallow donor to free-hole recombination; $g=(D^+,X)$ is the ionized donor bound-exciton transition; $h=(A^0,X)$ is the neutral acceptor bound-exciton transition; $i=(D_2^0,X)$ is the neutral deep-donor bound-exciton recombination; $j=(D^0,A^0)$ is the shallow donor-acceptor pair recombination.

$(F,X)_{n=1}$ transitions,[7] indicating a sample of very high purity. The different observed n components result from different angular momentum states of the $J=\frac{3}{2}$ hole characteristic of the valence-band maximum.[16] At low energy, the very weak intensity of the (A^0,X) transitions (structure h), indicates a sample with a low concentration of compensating impurities. Moreover, the small relative intensity ratio (≈ 0.02) between the (A^0,X) and $(D^0,X)_{n=1}$ transitions, indicates a low-compensation sample. These results are in qualitative agreement with the electrical transport analysis. At the low-energy end of the spectrum, a weak broad structure (structure i) is observed below the (A^0,X) transition. As shown in the inset of Fig. 6, structure i extends up to the high-energy side of the shallow donor-acceptor (D^0,A^0) pair recombinations (structure j). This indicates, in contrast to the sharp optical features observed for the $(D^0,X)_n$ lines ($\gamma_{(D^0,X)_n}$ in the range 0.04–0.07 meV), that structure i arises from a band rather than from a discrete energy level. In order to study the nature of the binding center responsible for the emission band centered at ≈ 1.4080 eV, PLE spectroscopy was performed at various energies on the emission band. PLE is a very powerful technique to differentiate between excitonic and nonexcitonic transitions. In Fig. 6, we have displayed the PLE spectrum of sample 1 with the spectrometer detection set at the center of structure i. A strong resonance is observed at the $(F,X)_{n=1}$ transition when the laser is tuned over the excitonic region, thereby resonantly creating excitons that are subsequently trapped on impurities. For nonexcitonic luminescence the PLE shows a dip at the energy of the $(F,X)_{n=1}$ transition, since the creation of excitons now creates a parallel recombination channel competing with nonexcitonic recombination.[19] The same results were obtained by locating the detection energy across the broad emission band. We thus attribute structure i to excitonic PL. Further information on the excitonic nature of structure i can be obtained from TRPL measurements. In Fig. 7, we display the PL decay measurements (open circles) of selected lines (a,e,i) shown in Fig. 6. All curves exhibit exponentially decaying behaviors characteristic of excitonic transitions. The solid lines represent least squares fit to the data yielding the following decay lifetimes $\tau_{(F,X)_{n=1}}=2.4$ ns, $\tau_{(D^0,X)_{n=1}}=2.5$ ns, $\tau_{\text{high}}=3.9$ ns, $\tau_{\text{mid}}=12.8$ ns, and $\tau_{\text{low}}=24.9$ ns, where the subscripts high, mid, and low are the energy ranges considered across the broad emission band. The decay lifetimes τ_d increase with increasing exciton localization energy $E_{B,X}$, as one would expect from general consideration of τ_d versus $E_{B,X}$. From the electrical transport analysis of Sec. III, we can invoke that deep-donor centers are responsible for the localization of the excitons across the luminescent band. The increase in τ_d can thus be understood qualitatively if the electron of the neutral deep donor becomes more localized with increasing $E_{B,X}$, leading to a decrease in electron-hole wave-function overlap, and thus to an increase in τ_d.[20] To further confirm the deep-donor binding energy E_{D_2} extracted from the electrical transport analysis, we have investigated the PL in

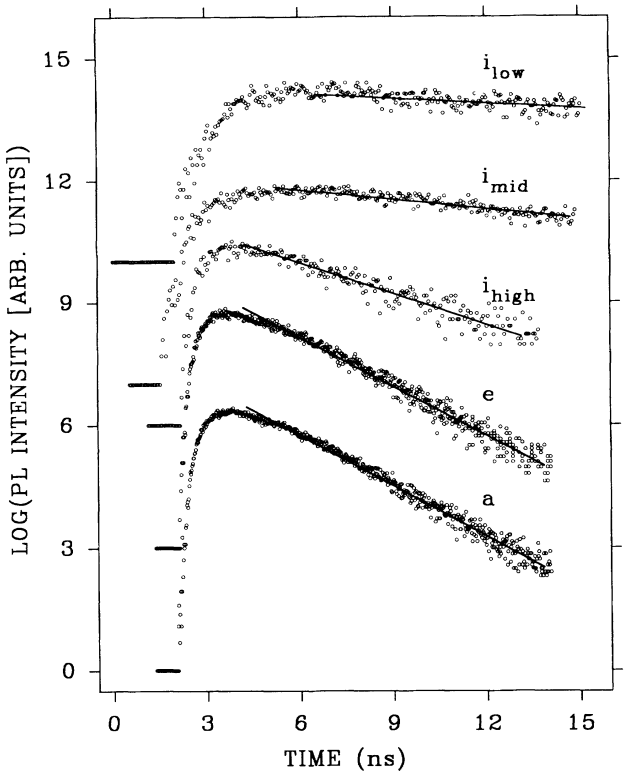

FIG. 7. Photoluminescence decay measurements (open circles) of selected lines shown in Fig. 6 under identical experimental conditions. The solid curves are least squares fit to the data. The decay lifetimes of lines a, e, i_{high}, i_{mid}, and i_{low} are, respectively, 2.4, 2.5, 3.9, 12.8, and 24.9 ns. The subscripts high, mid, and low stand for the energy ranges considered across the structure i of Fig. 6.

the spectral region corresponding to the deep donor-acceptor pair (D_2^0,A^0) recombinations. However, such transitions could not be observed owing to the low values of N_{D_2} and N_A quoted in Table II. Consequently, an estimate of E_{D_2} can only be obtained by considering the deep-donor bound-excitonic nature of structure i. Similarly to the case of deep acceptors in GaAs,[6] E_{D_2} has been estimated in a first approximation using $E_{D_2}=\xi^{-1}[h\nu_{(F,X)_{n=1}}-h\nu_{(D_2^0,X)}]$, where $h\nu_{(F,X)_{n=1}}=1.4189$ eV, $h\nu_{(D_2^0,X)}$ is the deep-donor bound-exciton photon energy observed to be within $\approx[1.4080\pm 2.5\gamma_{(D_2^0,X)}]$ eV where $\gamma_{(D_2^0,X)}\approx 11$ meV (see inset of Fig. 6), and $\xi=0.1$. The coefficient ξ gives a measure of the localization energy of the exciton to the deep-donor site, according to Haynes rule.[21] The resulting values of E_{D_2} extend from the edge of the conduction band to ≈ 390 meV below the conduction band. This result is consistent with the electrical transport analysis (see Table II for the extracted values of σ_{D_2}). Any discussion on the structural and chemical origin of this deep-donor band is at this point premature and highly speculative.

V. SUMMARY

In summary, we presented electrical and optical data of *n*-type InP grown by chemical-beam epitaxy supporting the presence of a broad band of localized deep donors, centered at 160 meV below the conduction band. The Hall mobility of the samples was found to be exceptionally high at 77 K and significantly reduced at 300 K. In addition, all the samples exhibited at the lowest temperatures an anomalous metal-like behavior, instead of the expected strong localization regime. Despite high quality and rich low-temperature photoluminescence optical features, the 77-K Hall mobility of the samples is not a sufficient criterion to assess their purity, as evidenced by the very strong electronic excitation to the conduction band in a broad temperature range ($\approx$35–300 K) and the corresponding low Hall mobility. A broad luminescent band of $\approx$11-meV linewidth linked to the presence of the band of deep donors was observed between the acceptor bound-exciton transition and the shallow donor-acceptor pair recombinations. Photoluminescence excitation as well as time-resolved photoluminescence measurements supported the bound-exciton nature of the luminescent band. Moreover, it can be invoked from a detailed electrical transport analysis that deep-donor centers or complexes are responsible for the exciton localization across the luminescent band. The binding energies of the deep-donor centers extracted from the optical measurements are consistent with the corresponding values deduced from the analysis of the electrical transport data.

---

*Also with the Département de Physique et Groupe de Recherche en Physique et Technologie des Couches Minces, Université de Montréal, Case Postale 6128, Succursale A, Montréal, Québec, Canada H3C 3J7.

†Visiting scientist.

[1]M Benzaquen, K. Mazuruk, and D. Walsh, Phys. Rev. B **36**, 4388 (1987).

[2]M. Benzaquen, M. Beaudoin, and D. Walsh, Phys. Rev. B **38**, 7824 (1988).

[3]M. Benzaquen, D. Walsh, M. Beaudoin, K. Mazuruk, and N. Puetz, J. Cryst. Growth **93**, 562 (1988).

[4]B. I. Shklovski and A. L. Efros, *Electronic Properties of Doped Semiconductors,* Springer Series in Solid-State Sciences Vol. 45 (Springer-Verlag, New York, 1984).

[5]H. Künzel and K. Ploog, Appl. Phys. Lett. **37**, 416 (1980).

[6]S. Charbonneau, W. G. Mcmullan, and M. L. W. Thewalt, Phys. Rev. B **38**, 3587 (1988).

[7]T. Sudersena Rao, C. Lacelle, R. Benzaquen, P. D. Berger, S. J. Rolfe, S. Charbonneau, A. P. Roth, T. Steiner, and M. L. W. Thewalt, J. Appl. Phys. (to be published).

[8]D. L. Rode, Phys. Rev. B **3**, 3287 (1971).

[9]D. L. Rode, Phys. Status Solidi B **55**, 687 (1973).

[10]H. Brooks, Phys. Rev. **83**, 879 (1951).

[11]A. R. Hutson, J. Appl. Phys. **32**, 3287 (1961).

[12]D. L. Rode, *Transport Phenomena,* edited by R. Willardson and A. Beer (Academic, New York, 1975), Vol. 10.

[13]C. Erginsoy, Phys. Rev. **79**, 1013 (1950).

[14]A. A. Grinberg, Fiz. Tekh. Poluprovodn. **12**, 657 (1978) [Sov. Phys. Semicond. **12**, 383 (1978)].

[15]N. Sclar, Phys. Rev. **104**, 1548 (1956).

[16]P. J. Dean and M. S. Skolnick, J. Appl. Phys. **54**, 346 (1983).

[17]R. H. Bube, *Electronic Properties of Crystalline Solids* (Academic, New York, 1975), Vol. 10, pp. 7–46.

[18]M. Benzaquen and D. Walsh, Solid State Commun. **89**, 1033 (1994).

[19]T. Steiner, Yu Zhang, S. Charbonneau, A. Villemaire, M. L. W. Thewalt, M. Maciaszek, and R. P. Bult, Can. J. Phys. **67**, 242 (1989).

[20]E. I. Rashba and G. E. Gurgenishvili, Fiz. Tverd. Tela (Leningrad **4**, 1029 (1962) [Sov. Phys. Solid State **4**, 759 (1962)].

[21]J. R. Haynes, Phys. Rev. Lett. **4**, 361 (1960).